Fixel-Based Analysis of Visual Pathway White Matter in Primary Open-Angle Glaucoma

Shereif Haykal,[1] Branislava Ćurčić-Blake,[2] Nomdo M. Jansonius,[3] and Frans W. Cornelissen[1]

[1]Laboratory for Experimental Ophthalmology, University of Groningen, University Medical Center Groningen, Groningen, The Netherlands
[2]Department of Biomedical Sciences of Cells & Systems, University Medical Center Groningen, Groningen, The Netherlands
[3]Department of Ophthalmology, University of Groningen, University Medical Center Groningen, Groningen, The Netherlands

Correspondence: Shereif Haykal, Laboratory for Experimental Ophthalmology, University Medical Center Groningen, PO Box 30.001, Groningen 9700 RB, The Netherlands;
s.a.m.m.haykal@umcg.nl.

Submitted: May 3, 2019
Accepted: August 10, 2019

Citation: Haykal S, Ćurčić-Blake B, Jansonius NM, Cornelissen FW. Fixel-based analysis of visual pathway white matter in primary open-angle glaucoma. *Invest Ophthalmol Vis Sci*. 2019;60:3803–3812. https://doi.org/10.1167/iovs.19-27447

Purpose. White matter (WM) degeneration of the visual pathways in primary open-angle glaucoma (POAG) is well documented, but its exact pathophysiology remains unclear. To date, glaucomatous WM degeneration has been exclusively studied using diffusion tensor imaging (DTI) only. However, DTI measures lack direct biological interpretation, and the approach itself suffers from multiple technical limitations. Fixel-based analysis (FBA) is a novel framework for studying WM degeneration, overcoming DTI's technical limitations and providing biologically meaningful metrics. FBA measures fiber density (FD), representing early microstructural changes, and fiber-bundle cross section (FC), representing late macrostructural changes. In this study, we use FBA to study glaucomatous degeneration of the pregeniculate optic tracts (OTs) and postgeniculate optic radiation (ORs) in POAG.

Methods. This was a cross-sectional case-control study with 12 POAG patients and 16 controls. Multi-shell diffusion-weighted images were acquired. FBA was used to produce a population template, and probabilistic tractography was used to track the OTs and ORs in template space. Finally, FD and FC of the tracts of interest were compared between the two groups.

Results. Compared with the controls, the OTs of the patients exhibited a significant (familywise error corrected $P < 0.05$) decrease in FD and FC, whereas their ORs exhibited a significant decrease in FD but not in FC.

Conclusions. FBA provides sensitive measures to assess WM changes in glaucoma. Our findings suggest that the OTs of glaucoma patients exhibit signs of more advanced WM degeneration compared with the ORs. This potentially implicates anterograde trans-synaptic propagation as the primary cause of glaucomatous spread along the visual pathways.

Keywords: glaucoma, primary open-angle glaucoma, magnetic resonance imaging, diffusion-weighted imaging, fixel-based analysis

Primary open-angle glaucoma (POAG) is one of the leading causes of irreversible blindness worldwide, and its prevalence is only expected to increase as the world's population continues to age.[1] POAG results in the death of retinal ganglion cells (RGCs), leading to thinning of the retinal nerve fiber layer (RNFL) and loss of peripheral vision.[2] Furthermore, glaucomatous degeneration of the visual system beyond the retina has been documented in experimental animal models,[3–7] postmortem human histopathologic studies,[8] and human neuroimaging studies.[9–11] Such studies have found evidence of glaucomatous degeneration in the lateral geniculate nucleus (LGN) and the visual cortex, suggesting the involvement of the brain in glaucomatous disease pathology.[12] However, neither the cause nor the origin of this degeneration is fully understood.

Trans-synaptic spread is one of the proposed explanations of glaucomatous degeneration of the central visual system.[13] The conventional view of POAG as simply a degenerative retinal disease implicates anterograde trans-synaptic degeneration in glaucomatous spread, as degeneration would start at the pregeniculate RGCs and spread across the LGN to reach the postgeniculate pathways. However, a small number of primate studies have found evidence of LGN degeneration preceding RGC loss,[5,14] suggesting a retrograde trans-synaptic spread. Furthermore, some MRI studies of POAG patients have reported degenerative changes outside the visual system.[15–17] This has led to the suggestion that an independent brain component may be present in POAG and potentially implicates retrograde trans-synaptic degeneration as a cause of RGC degeneration.

As the visual pathway is uniquely divided into two major white matter (WM) tracts (pre- and postgeniculate), investigating glaucomatous WM degeneration potentially holds the key to understanding the true nature of glaucomatous neurodegenerative spread across the visual system. To date, the most commonly used method for studying WM degeneration in POAG patients has been diffusion tensor imaging (DTI).[15–36] However, DTI metrics have no direct biological interpretation and are commonly interpreted as estimates of WM "structural integrity." Furthermore, DTI has technical limitations, most notably its inability to account for crossing-fibers within the same voxel.[37] Therefore, several higher-order diffusion models have been recently developed to overcome these limitations and to produce more biologically meaningful measures.[38–45]

Fixel-based analysis (FBA) is a recently proposed framework that uses such a higher-order model for analyzing WM in a fiber population–specific manner.[45] The term fixel refers to a specific fiber population within a voxel. FBA uses constrained spherical deconvolution (CSD)[40,44] to model multiple fiber orientations within the same voxel, allowing for the disentanglement of differently oriented WM fiber populations (or fixels). By doing so, FBA solves the classic crossing-fibers problem encountered with DTI and produces biologically meaningful metrics for studying WM changes in vivo. These metrics are as follows: fiber density (FD), fiber-bundle cross section (FC), and fiber density and bundle cross section (FDC). FD represents intra-axonal volume of separate fiber populations within each voxel.[45] FD can be used to probe WM microstructural changes in a fiber-specific manner, with a decrease in FD indicating a loss of axons.[45,46] FC quantifies gross morphologic (or macrostructural) WM changes by measuring fiber bundle cross-sectional area in a plane perpendicular to fixel orientation.[45,46] Finally, FDC is a combined measure of both FD and FC, providing a more comprehensive measure of the information carrying capacity of fiber tracts.

In this study, we use FBA to investigate WM changes in the pregeniculate optic tracts (OTs) and the postgeniculate optic radiations (ORs) in POAG to better understand the underlying pathophysiology of glaucomatous neurodegeneration. Furthermore, we investigate the correlation between FBA metrics and structural and functional clinical measures of glaucoma. Finally, for comparison, we analyze the same tracts using the conventional voxelwise DTI approach.

Methods

Ethical Approval

This study was approved by the ethics board of the University Medical Center Groningen (UMCG). All participants provided written informed consent before participation. The study adhered to the tenets of the Declaration of Helsinki.

Participants

Eighteen glaucoma patients and 18 controls volunteered to participate. All glaucoma patients were recruited from the UMCG. Inclusion criteria for the controls were as follows: having intact visual fields, an IOP $\leq$ 21 mm Hg, and a visual acuity of 0.8 or higher (+0.1 logMAR or less) in both eyes. Exclusion criteria for both groups were as follows: having any ophthalmic disorder affecting visual acuity or visual field (apart from POAG in glaucoma group), a history of any neurologic or psychiatric disorders, the presence of gross abnormalities or lesions in their magnetic resonance imaging (MRI) scans, or having any contraindication for MRI (e.g., having a pacemaker or being claustrophobic). Six glaucoma participants were excluded for having non-POAG subtypes of glaucoma (namely pseudoexfoliative glaucoma and pigmentary glaucoma). Two controls were excluded, one for having a history of a transient ischemic attack and cognitive impairment and the other for having an IOP > 21 mm Hg. In total, 12 POAG patients and 16 controls were included in this cross-sectional study. Demographics of included participants are listed in Table 1.

Ophthalmic Data

All subjects underwent tests for visual acuity, IOP, visual fields, and retinal nerve fiber layer (RNFL) thickness.

Visual acuity was measured using a Snellen chart with optimal correction for the viewing distance. IOP was measured using a Tonoref noncontact tonometer (Nidek, Hiroishi, Japan). Visual fields for the POAG group were assessed using a Humphrey Field Analyzer (HFA; Carl Zeiss Meditec, Jena, Germany) using the 30-2 grid and the Swedish Interactive Threshold Algorithm (SITA), and expressed as visual field mean deviation (VFMD). For the controls, visual fields were screened using frequency doubling technology (FDT; Carl Zeiss Meditec) using the C20-1 screening mode. Controls were not allowed to have any reproducibly abnormal test location at $P < 0.01$. Finally, the RNFL thickness was measured by means of optical coherence tomography (OCT) using a Canon OCT-HS100 scanner (Canon, Tokyo, Japan). Results were expressed as the mean peripapillary RNFL (pRNFL) thickness.

Table 1. Group Demographics and Clinical Characteristics

Characteristics	POAG ($n = 12$)	Controls ($n = 16$)	Group Difference P
Age (y)	67.3 (7.3)	69.1 (7.3)	0.51
Male sex	6 (50%)	10 (62.5%)	0.51
Pretreatment IOP* (mm Hg)	34.1 (13.1)		
IOP recorded during study (mm Hg)			
Right	12.9 (3.3)	12.3 (3.1)	0.604
Left	13.0 (4.7)	13.0 (3.7)	0.832
pRNFL thickness (μm)			
Right	71.3 (10.1)	97.3 (7.9)	<0.001
Left	70.8 (12.7)	97.8 (8.5)	<0.001
VFMD (dB)			
Better eye	−3.3 (5.1)		
Worse eye	−14.5 (9.7)		

Values are presented as mean (SD) or number (%). VFMD measures where acquired in the POAG group only.

* Reported values for the POAG group are of the eye with higher pretreatment IOP.

Image Acquisition and Preprocessing

Diffusion-weighted images were acquired using a Siemens MAGNETOM Prisma 3T MRI scanner (Siemens, Erlangen, Germany) with a 64-channel head coil. The following parameters were used: repetition time (TR) = 5500 ms, echo time (TE) = 85 ms, bandwidth = 2404 Hz, field of view (FoV) = 210 × 210 × 132, voxel size = 2.0 × 2.0 × 2.0 mm, 66 slices, in 64 diffusion gradient directions. Two DWI shells were acquired, b = 1000 s/mm^2 and b = 2500 s/mm^2, in two phase encoding directions: anteroposterior and posteroanterior. Three images with no diffusion weighting (b = 0 s/mm^2) were also acquired in each phase encoding direction.

DWI preprocessing included first denoising the data[47] in MRtrix3 (www.mrtrix.org) and then correction of EPI distortions,[48] motion, and Eddy-current distortions[49] in FSL v5.011.[50]

FBA

Unless specified otherwise, the recommended FBA pipeline[45] was followed. All FBA steps, summarized below, were performed in MRtrix3.

First, the preprocessed DWI data were upsampled to a voxel size of 1.3 mm isotropic. Then, using a group average response function,[51] fiber orientation distributions (FODs) were estimated for each subject using the Multi-Shell Multi-Tissue Constrained Spherical Deconvolution (MSMT-CSD) algorithm.[52] Joint bias field correction and global intensity

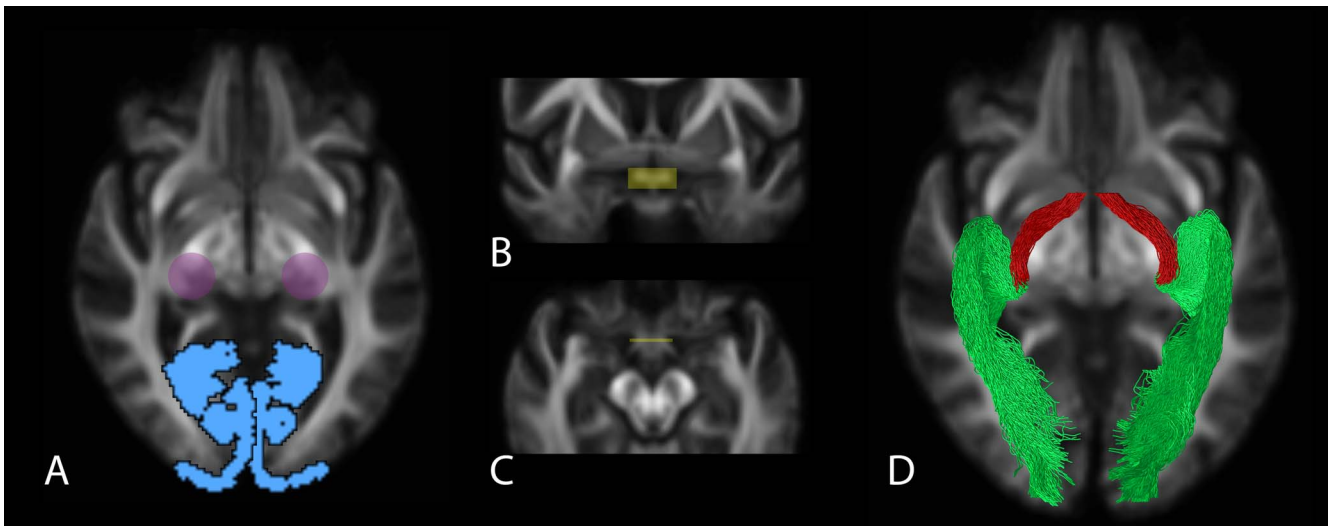

FIGURE 1. Probabilistic tractography of visual pathways using population template. (**A**) Regions of interest (ROIs) used for optic radiation fiber tracking. ROIs are overlaid on a representative axial slice. *Blue*, V1 masks; *magenta*, approximate visual representation of lateral geniculate nucleus ROIs. (**B**) Optic chiasm (OC) ROI (*yellow*) overlaid on a cropped coronal slice. (**C**) OC ROI overlaid on a cropped axial slice. (**D**) Tracked optic tracts (*red*) and optic radiations (*green*) overlaid on a representative axial slice.

normalization of the three different tissue compartments was then performed.[43]

A study-specific population FOD template was produced by iterative nonlinear registration and averaging of the FODs of all 28 subjects.[53] Subsequently, all FODs were nonlinearly registered to the average population template.[53,54] Then, the FODs were segmented to produce fiber-specific fixels within each voxel, and the produced fixels were then reoriented using the nonlinear registration warps produced earlier for each corresponding voxel. Finally, FBA metrics (FD, FC, and FDC) were calculated for each produced fixel.

A whole-brain probabilistic tractogram was produced using the FOD population template to identify local connectivity between neighboring fixels to enable the use of connectivity-based fixel enhancement[55] for statistical analysis. First, 20 million streamlines were generated, which were then filtered down to 2 million streamlines using the spherical-deconvolution informed filtering of tractograms (or SIFT)[56] approach to reduce biases in tractogram densities.

Visual Pathway Fiber Tracking

To study WM changes specifically in the visual pathways, we performed probabilistic tractography of the OTs and ORs using the population FOD template in MRTrix3.

OR fibers were tracked between the LGN and the primary visual cortex (V1) (Fig. 1A). Both LGNs were identified manually on the FOD template, guided by the generated whole-brain tractogram, and then 4-mm spherical regions of interest (ROIs) were used to circumscribe their approximate location. Left and right V1 masks were first created in MNI space using Freesurfer cortical parcellation of the MNI template (https://surfer.nmr.mgh.harvard.edu). The V1 masks were then transformed to the FOD template space nonlinearly using FMRIB's Non-linear Image Registration Tool (FNIRT) in FSL. Finally, 5000 streamlines were generated for each OR using the LGN ROI as a seed point and the V1 mask as an inclusion ROI (Fig. 1D). Fiber tracking was anatomically constrained using masks of nonthresholded OR probability maps derived from the Jülich histologic Atlas in FSL[57] to exclude streamlines that do not anatomically conform to the ORs.

OT fibers were tracked between the LGN and the optic chiasm (OC). To ensure that the tracked OT fibers passed through the OC, an ROI was manually created in the coronal plane corresponding to the middle of the OC, ensuring that all of the OC cross-sectional area in that plane was covered by the ROI (Figs. 1B, 1C). This resulted in a rectangular ROI measuring $6 \times 14 \times 1$ voxels (or $7.8 \times 18.2 \times 1.3$ mm). The same LGN ROIs used for OR tracking were used as seed ROIs, and the OC ROI was used as an inclusion ROI. Five hundred streamlines were generated for each OT between the LGN and OC ROIs (Fig. 1D).

The generated OT and OR tractograms were then converted to fixel masks to allow tract-of-interest analysis in a fixelwise manner within the FBA framework.

DTI Voxel-Based Analysis

In addition to FBA, we investigated changes in the visual pathways using the traditional DTI voxel-based approach as well. Using the preprocessed diffusion-weighted images, tensor-derived[58] FA and MD parametric maps were produced from the $b = 0$ s/mm^2 and $b = 1000$ s/mm^2 shells in the native space of each subject. Then, the FA and MD maps were nonlinearly registered to the FOD population template using the subject-to-template warps produced earlier to register individual FODs to the population template for FBA. To allow tract-specific DTI analysis, voxel masks were created from the OT and OR tractograms. All steps were performed in MRTrix3.

Statistical Analysis

Fixelwise statistical analysis was applied to the fixels included in the OT and OR fixel masks. A general linear model (GLM) was used to compare FD, FC, and FDC between the POAG group and the controls. Sex and demeaned age were added as nuisance covariates. Connectivity-based fixel enhancement was used to perform tract-specific smoothing and enhancement using the default parameter settings.[55] Following 5000 permutation tests, each fixel was assigned a familywise error (FWE) corrected *P* value. Streamline segments corresponding to statistically significant fixels were cropped from the

population template whole-brain tractogram and used to visualize significant results.

To further analyze our findings, the average FD, FC, and FDC of each tract was calculated for all participants. The average FBA metrics of each tract of the two groups were then compared using analysis of covariance (ANCOVA), adding age and sex as nuisance covariates. To study the correlation between the FBA metrics and the clinical glaucoma tests, the FD and FC of both sides of the OTs and ORs were averaged for each glaucoma patient. Then, a partial Pearson test was used to determine the correlation between the average pRNFL thickness and VFMD of both eyes and the averaged FBA metrics of the OTs and ORs, while controlling for the effects of age and sex.

For voxel-based DTI analysis, threshold-free cluster enhancement and permutation testing was performed in MRTrix3 using the provided default parameters.[59] FA and MD of the OTs and ORs were tested in a voxelwise manner using the same design matrix created for the FBA.

To compare participants' demographics and clinical characteristics, an independent-samples *t*-test was used for parametric continuous variables of equal variance, the Mann–Whitney *U* test was used for nonparametric continuous variables, Welch's *t*-test was used for continuous variables of unequal variance, and the χ^2 test was used for categorical variables.

Statistical significance for FBA and DTI analysis was reported at an FWE-corrected $P < 0.05$. For other tests, statistical significance was reported at $P < 0.05$.

Results

To summarize our results, FBA of the OTs revealed a significant loss of FD, FC, and FDC in the POAG group compared with controls, whereas the ORs showed a significant decrease in FD and FDC only. For glaucoma patients, FD of the OTs showed a significant correlation with the pRNFL thickness and VFMD, whereas FD of the ORs showed a significant correlation with pRNFL thickness only. FC measures of both OTs and ORs did not show any significant correlation with pRNFL thickness or VFMD. Using conventional DTI, the POAG group showed a significant decrease of FA in both OTs and the left OR, whereas a significant increase in MD was found in the OTs only. These results are described in more detail below.

Demographics and Clinical Characteristics

Table 1 summarizes the demographic and clinical characteristics of the two groups. They did not differ significantly in age, sex, or IOP. pRNFL thickness was significantly lower in the POAG group. Based on the Hodapp-Parrish-Anderson (H-P-A) classification[60] of the worse eye, the POAG group comprised three early stage, two moderate, three advanced, and four severe POAG patients. Supplementary Table S1 lists the pRNFL thickness, VFMD, and H-P-A staging of each eye of the 12 POAG patients. Supplementary Figure S1 illustrates cumulative VFMD maps for the left eye, right eye, and their binocular average for the POAG patients.

Fixel-Based Analysis of the Visual Pathways

Figure 2 illustrates fiber-specific results of the FD metric. The enlarged insets highlight the presence of crossing fibers in the ORs and lack thereof in OTs. Streamline segments corresponding to significant fixels of all three FBA metrics in the OTs and ORs are displayed in Figure 3. Comparison of the average FBA metrics of the OTs and ORs between POAG patients and controls can be found in Supplementary Table S2.

FBA of the OTs revealed significant loss of FD, FC, and FDC in the POAG group compared with the controls. All three metrics displayed a comparable bilateral spatial distribution of significant fixels along the length of the OTs. The ORs, on the other hand, showed a significant loss of FD and FDC only, whereas no significant difference in FC could be detected between the two groups. The left OR displayed a more spatially pervasive pattern of FD and FDC loss compared with the right OR.

Correlation Between FBA Metrics and Clinical Glaucoma Tests

FD of the OTs of glaucoma patients showed a significant correlation with the average pRNFL thickness and VFMD ($r^2 = 0.77$, $P < 0.01$ and $r^2 = 0.57$, $P < 0.05$, respectively), whereas FD of the ORs showed a significant correlation with pRNFL thickness only ($r^2 = 0.41$, $P < 0.05$). FC of both OTs and ORs showed no significant correlation with neither of the clinical tests. Table 2 lists the results of all performed correlation tests.

Tensor-Based Analysis of the Visual Pathways

A significant decrease in FA was found bilaterally in the OTs in POAG, whereas only the left OR showed a significant decrease in FA. Significant voxels were evenly distributed along both OTs, whereas the left OR exhibited a cluster of 12 significant voxels mid-pathway (Fig. 4). The POAG group showed a significant increase in MD along both OTs, whereas their ORs showed no significant difference compared with the controls (Fig. 4).

Discussion

The main findings of this study are that, in POAG patients, OTs exhibit both micro- and macrostructural degeneration, whereas ORs show evidence of microstructural degeneration only. To the best of our knowledge, this is the first study to use FBA to investigate WM degeneration in POAG. We find that FBA is more sensitive to glaucomatous degeneration in the ORs compared with conventional DTI, highlighting the importance of adopting higher-order diffusion models for studying glaucomatous WM changes. We describe these conclusions in more detail.

Distinct Patterns of FBA Changes in Visual Pathways in POAG

The OTs of POAG patients exhibited a decrease in both FD and FC, implying a loss of axons and atrophy of fiber bundles compared with the controls. On the other hand, the ORs exhibited a decrease in FD only, implying a loss of axons with no accompanying loss in fiber bundle size. The ORs also demonstrated a decrease of FDC in overlapping regions of FD loss. This confirms that the decrease of FD in the ORs reflects true axonal loss in the absence of fiber bundle atrophy, as an alteration in FC would have resulted in a discrepancy between regions of FD and FDC loss.

A possible interpretation of the difference in fiber bundle atrophy between the OTs and ORs, in the presence of axonal loss in both the OTs and ORs, is that OTs manifest more advanced glaucomatous degeneration compared with ORs. Generally, the earliest sign of WM degeneration is axonal loss, which leaves the extra-axonal space filled with axonal debris

Investigative Ophthalmology & Visual Science

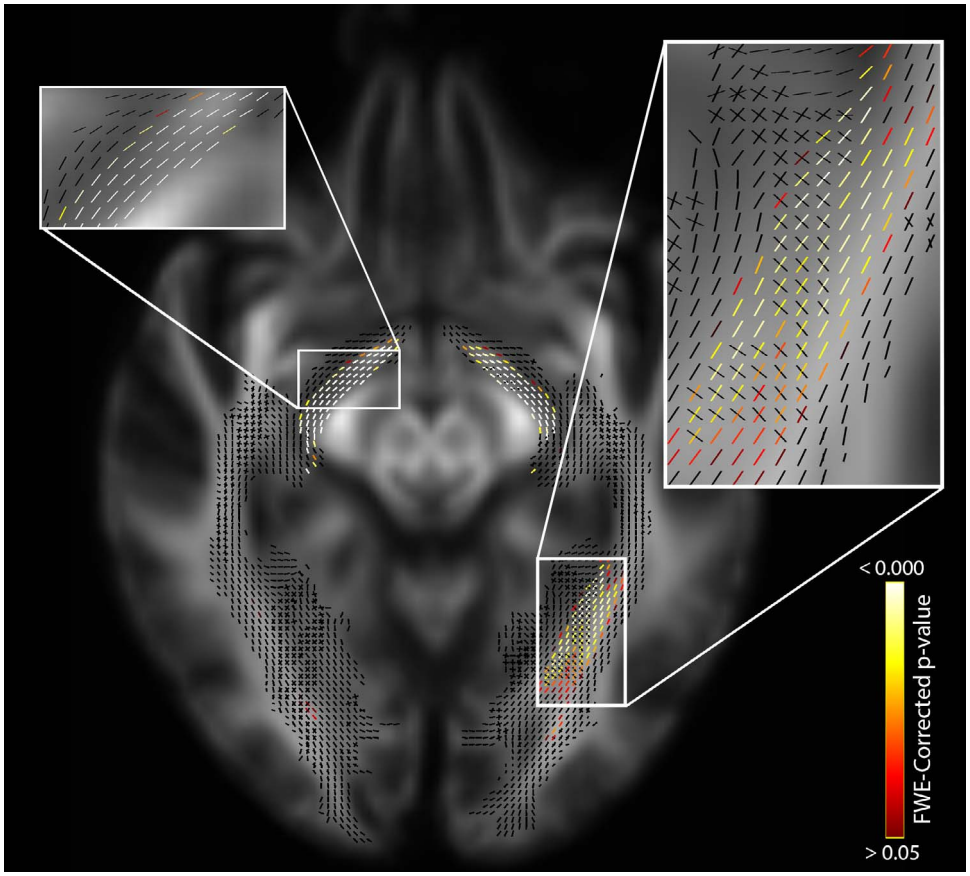

Figure 2. Fixel-based analysis of FD along the visual pathways. Fixels exhibiting statistically significant FD loss in POAG group compared with controls are color-coded by their assigned FWE-corrected *P* value, whereas nonsignificant fixels are shown in black. Results are shown for a single axial slice displayed in radiological convention. Zoomed-in regions show a closer view of the fixels in the right optic tract and left optic radiation.

and inflammatory and glial cells.[61] Eventually, as the debris is cleared and the inflammatory reaction subsides, WM starts exhibiting gross atrophic changes. This chronologic sequence of degenerative WM changes has been previously described in an animal study of time-dependent morphologic changes in glaucoma monkey models, where loss of ON axons was shown to precede the decrease in ON cross-sectional area.[6] Therefore, based on our knowledge of WM changes along the time course of glaucomatous neurodegeneration, the results of this study potentially suggest that the pregeniculate pathways of glaucoma patients show evidence of more advanced stages of degeneration compared with postgeniculate pathways. This pattern of WM degeneration corresponds with anterograde trans-synaptic spread along the visual pathway, starting pregeniculately and propagating downstream toward the visual cortex. It should be noted that our study population had a mean pretreatment IOP much greater than 21 mm Hg. In normal tension glaucoma, the underlying pathophysiology and degeneration pattern could be different.

Correlation With Structural and Functional Clinical Tests

The pRNFL thickness showed a stronger correlation with the FD of both the OTs and ORs than did the VFMD. This is expected, as both FD and pRNFL thickness are measures of structural degeneration, whereas VFMD is a measure of functional loss. Additionally, the FD of the OTs showed a stronger correlation with both clinical measures compared with the FD of the ORs. This could be attributed to the fact that the clinical tests examine the structure and function of the optic nerves, which are essentially formed of the same RGCs axons as the OTs. Furthermore, the FC of both tracts was not correlated with either of the clinical measures. A possible explanation for this lack of correlation is that FC changes, unlike FD and structural and functional optic nerve changes, are a delayed secondary outcome of axonal loss and not a direct response to it. This further strengthens our assertions regarding the time course of micro- and macrostructural WM changes in POAG.

Surprisingly, the average VFMD maps (Supplementary Fig. S1) failed to explain the difference in spatial pervasiveness of FD loss between the left and right ORs. A similar (unexplained) difference has been previously reported in a meta-analysis of DTI studies of glaucoma,[62] although the meta-analysis found a greater decrease of FA on the right side.

FBA Is More Sensitive to Glaucomatous Degeneration Than DTI

In agreement with our FBA results, the DTI analysis revealed a decrease in FA and an increase in MD along the entire length of both OTs in the POAG group (Fig. 4), indicating widespread bilateral degeneration. However, in contrast to the FBA results, the left OR exhibited a decrease of FA in a relatively small cluster of 12 voxels only, whereas the right OR showed no significant difference in FA or MD.

The discrepancy between FBA and DTI results could be partly explained by the difference in the anatomical surroundings of the OTs and ORs. The OTs are surrounded by CSF of the

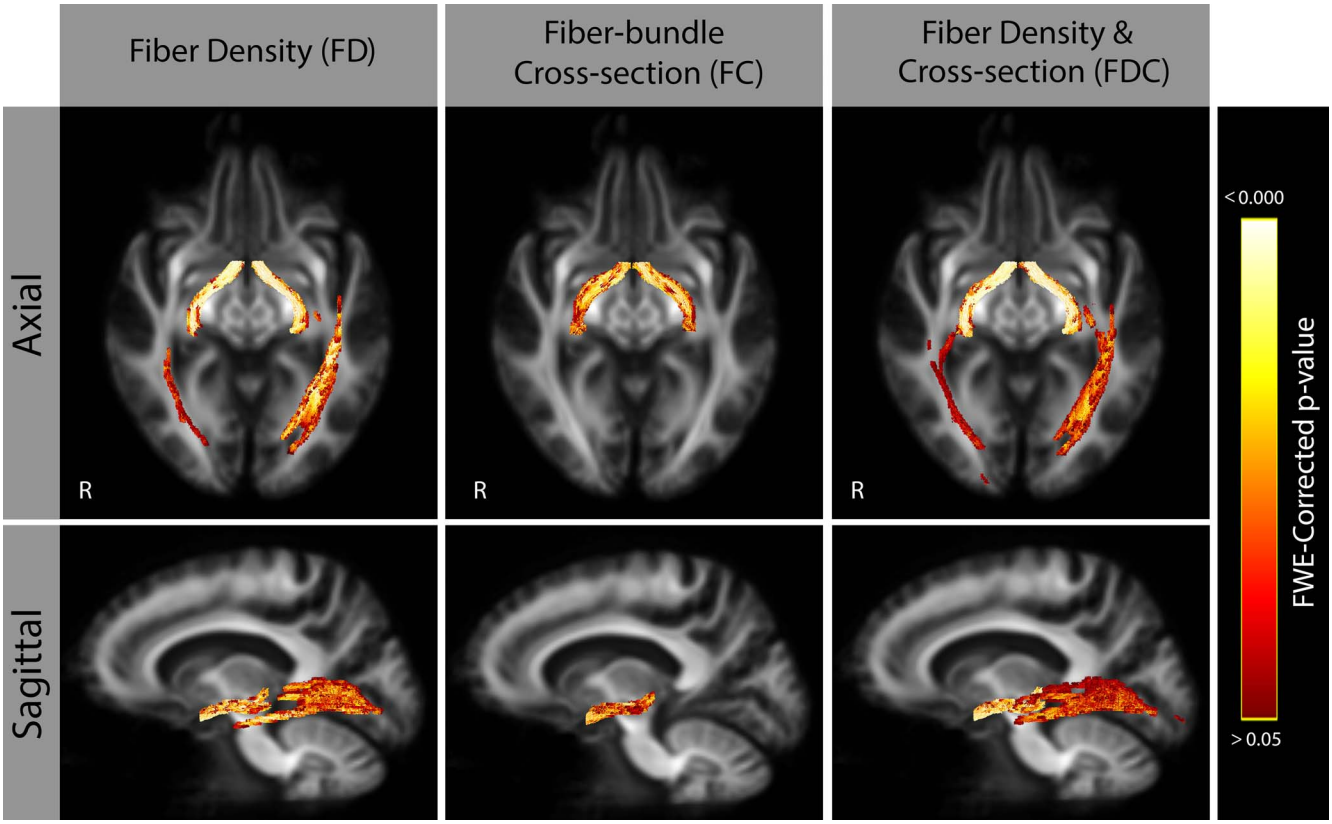

Figure 3. Decreased fixel-based metrics in the visual pathways in POAG. Fixels in the optic tracts demonstrated a significant loss of FD, FC, and FDC in the POAG group compared with controls. Fixels in the optic radiations demonstrated a significant loss of FD and FDC only. Streamlines corresponding to fixels with a significant reduction are overlaid on representative axial and sagittal slices from the population template. Images are displayed in radiologic convention.

perimesencephalic cisterns for most of their length. This reduces the possibility of crossing-fibers from other WM tracts being present within the same voxel and hence enables DTI to measure changes in diffusivity in OTs voxels. The ORs, on the other hand, are surrounded by other cerebral WM bundles, resulting in the presence of crossing and so-called "kissing" fibers within the same voxels.[63–65] DTI is incapable of modeling such crossing fibers, limiting its ability to analyze regions of complex WM structure of the ORs. FBA overcomes this limitation, as it distinguishes between different fiber orientations within the same voxel. Figure 2 illustrates the prevalence of crossing fibers in the ORs and lack thereof in OTs and demonstrates the ability of FBA to analyze different crossing fiber populations independently.

Although DTI and FBA are not directly comparable techniques, our findings indicate that FBA is more suitable for studying glaucomatous neurodegeneration, in particular in the ORs. Moreover, DTI measures such as FA and MD provide limited understanding, as they lack direct biological interpretation. Our use of the novel FBA framework allowed us to gain more insight into the biological changes underlying the glaucomatous WM degeneration, both on a micro- and macro-scale.

Table 2. Correlation Between FBA Metrics and Clinical Glaucoma Tests

FBA Metric	Visual Tract	Correlation With pRNFL Thickness		Correlation With VFMD	
		Partial r^2	*P*	Partial r^2	*P*
FD	OT	0.77	0.001	0.41	0.047
	OR	0.57	0.012	0.25	0.137
FC	OT	0.06	0.513	0.32	0.089
	OR	0.20	0.195	0.30	0.103

Comparison to Previous Studies of WM Changes in POAG

Previous studies of visual pathway WM in POAG patients found evidence of degeneration in both the OTs and ORs using DTI.[62] However, very little can be concluded about the nature of this reported WM degeneration, as DTI metrics represent an all-encompassing measure of WM "structural integrity."

Several whole-brain DTI studies of POAG reported WM degeneration outside the visual system.[15–17,66] This implies the involvement of a global degenerative brain component in POAG. As such global degeneration can reach the RGCs only through retrograde trans-synaptic spread; this would contradict our interpretation of a possible predominance of anterograde trans-synaptic degeneration. Notably, most whole-brain DTI studies that reported evidence in favor of degeneration beyond the visual system used somewhat lenient statistical thresholds. For example, Frezzotti et al.[15,16] and Giorgio et al.[66] reported results from tract-based spatial statistics (TBSS) without correcting for multiple comparisons. Whole-brain studies that applied more stringent statistical thresholds found no evidence of WM degeneration outside the visual system.[25,35,67] Hence, we believe the evidence for a global degenerative brain component in POAG is relatively weak at best, whereas our present evidence for suggesting anterograde trans-synaptic

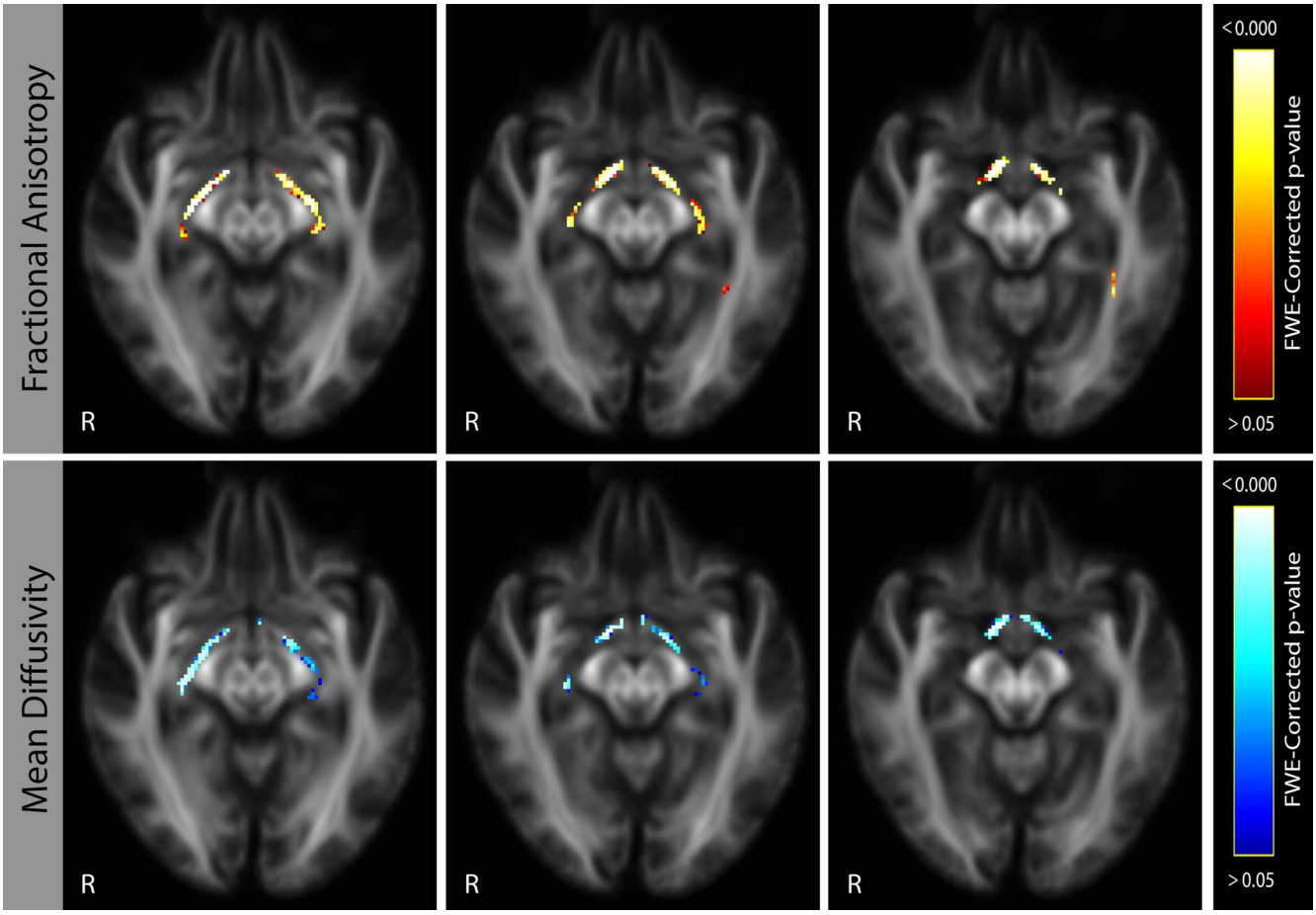

FIGURE 4. Voxel-based analysis showing differences in fractional anisotropy (FA) and mean diffusivity (MD) in the visual pathways in POAG. Voxels showing a significant increase of FA or a significant decrease of MD in POAG group are displayed across three sequential axial slices. *Top row*: Both optic tracts exhibited a significant decrease of FA, whereas the left optic radiation showed a cluster of 12 voxels with a significant decrease and the right optic radiation exhibited no voxels with a significant decrease. *Bottom row*: Both optic tracts exhibited a significant increase of MD, whereas both optic radiations showed no significant decrease of MD. Images are displayed in radiologic convention.

degeneration is comparatively strong. Therefore, the notion of an independent global component contributing to POAG may have to be reconsidered.

Regarding our results using the DTI approach, the lack of significant difference of FA in the right OR and of MD in both ORs, which has been reported in previous DTI studies, can be ascribed to multiple factors. First, our study included a relatively moderate sample size. Second, the inclusion of multiple patients with early-stage glaucoma (Supplementary Table S1) may have resulted in a relatively small effect size of DTI changes. Finally, our use of stringent FWE correction may have also played a role, as other DTI studies with larger sample sizes have failed to find any significant results following correction for multiple comparisons.[16]

Clinical Implications

Our current study contributes to understanding the underlying pathophysiology of visual pathway WM structural changes in POAG and how to best detect these changes, which could have crucial implications for the clinical management of glaucoma patients in the future.

Previous studies suggested the use of DWI for monitoring glaucoma progression and response to treatment. This idea has always been proposed in a theoretical capacity, as MRI scans are quite expensive and cumbersome compared with the currently used ophthalmic instruments. Based on our interpretation that glaucomatous visual pathway WM changes are potentially caused by anterograde trans-synaptic degeneration originating from the eye, our study supports the current practice of using OCT for fast and relatively inexpensive glaucoma assessment. Nevertheless, DWI could be used for monitoring glaucoma progression in patients for whom OCT might not be ideal, especially in late-stage glaucoma patients, where OCT fails to detect deterioration following a significant visual field defect.[68] Having more sensitive DWI analysis methods such as FBA available brings such clinical translation a step closer to practical application.

Studying glaucomatous WM changes could also play a role in the development of novel treatments. For example, newly developed neuroprotective treatments that aim to halt the progression of neurodegeneration[69,70] will need to take into account the degeneration occurring not only at the level of the retina but also throughout the visual system. Furthermore, novel therapies that aim to restore vision will need to consider the state of the entire visual pathway and not solely that of the retina. For example, RGC transplantation is currently being investigated as a treatment option for POAG.[71] A degenerated postgeniculate visual pathway would render such transplants useless, as the connection of the transplanted RGCs to the visual cortex would be interrupted. Therefore, understanding the nature of visual pathway glaucomatous degeneration and

how to best detect it would be essential for developing such novel treatments.

Limitations and Future Directions

The main limitation of this study is that our interpretations regarding the nature of glaucomatous spread along the visual pathways are based on cross-sectional data. The OTs and ORs differ considerably in size and shape, which means they might exhibit different patterns of FBA changes independent of the effect of glaucomatous degeneration. Although FBA metrics describe distinct aspects of WM degeneration, which we used as potential surrogate biomarkers for glaucomatous degenerative advancement, evidence of actual disease progression over time is still needed to confirm our findings.

Another study limitation is the relatively moderate sample size of our POAG group. However, finding statistically significant changes despite this sample size and while following rigorous correction for multiple comparisons is a testament to how sensitive FBA is to glaucomatous WM changes.

In this study, we set a precedent for the use of FBA in investigating POAG, and potentially other diseases that may affect the integrity of the visual pathways. Future studies with larger sample sizes and a longitudinal nature are required to verify our present suggestion that visual pathway WM changes are primarily caused by anterograde trans-synaptic degeneration originating from the eye.

Conclusions

FBA provides a sensitive technique for studying WM changes in glaucoma. Although previous DTI studies of POAG reported a nonspecific loss of structural integrity of the OTs and ORs, the current FBA study characterized these changes in a biologically meaningful manner. Our FBA findings suggest that the OTs of POAG patients exhibit signs of a more advanced stage of WM degeneration compared with the ORs, potentially implicating anterograde trans-synaptic propagation as the primary cause of glaucomatous spread along the visual pathways. These novel findings contribute to our understanding of the underlying pathophysiology of WM changes in POAG and could potentially lead to the advancement of POAG diagnostics and therapies in the future.

Acknowledgments

Supported by the Graduate School of Medical Sciences (GSMS), University of Groningen, Groningen, The Netherlands (SH). This project has received funding from the European Union's Horizon 2020 research and innovation programme under Marie Sklodowska-Curie Grant 675033 (Egret-plus). The funding organizations had no role in the design, conduct, analysis, or publication of this research.

Disclosure: **S. Haykal**, None; **B. Ćurčić-Blake**, None; **N.M. Jansonius**, None; **F.W. Cornelissen**, None

References

1. Tham YC, Li X, Wong TY, Quigley HA, Aung T, Cheng CY. Global prevalence of glaucoma and projections of glaucoma burden through 2040: a systematic review and meta-analysis. *Ophthalmology*. 2014;121:2081–2090.
2. Weinreb RN, Khaw PT. Primary open-angle glaucoma. *Lancet*. 2004;363:1711–1720.
3. Yucel YH, Zhang Q, Gupta N, Kaufman PL. Loss of neurons in magnocellular and parvocellular layers of the lateral geniculate nucleus in glaucoma. *Arch Ophthalmol*. 2000;118:378–384.
4. Weber AJ, Chen H, Hubbard WC, Kaufman PL. Experimental glaucoma and cell size, density, and number in the primate lateral geniculate nucleus. *Invest Ophthalmol Vis Sci*. 2000; 41:1370–1379.
5. Yücel YH, Zhang Q, Weinreb RN, Kaufman PL, Gupta N. Atrophy of relay neurons in magno-and parvocellular layers in the lateral geniculate nucleus in experimental glaucoma. *Invest Ophthalmol Vis Sci*. 2001;42:3216–3222.
6. Ito Y, Shimazawa M, Chen YN, et al. Morphological changes in the visual pathway induced by experimental glaucoma in Japanese monkeys. *Exp Eye Res*. 2009;89:246–255.
7. Yücel YH, Gupta N, Kalichman MW, et al. Relationship of optic disc topography to optic nerve fiber number in glaucoma. *Arch Ophthalmol (Chicago, Ill 1960)*. 1998;116: 493–497.
8. Gupta N, Ang LC, De Tilly LN, Bidaisee L, Yücel YH. Human glaucoma and neural degeneration in intracranial optic nerve, lateral geniculate nucleus, and visual cortex. *Br J Ophthalmol*. 2006;90:674–678.
9. Boucard CC, Hernowo AT, Maguire RP, et al. Changes in cortical grey matter density associated with long-standing retinal visual field defects. *Brain*. 2009;132:1898–1906.
10. Hernowo AT, Boucard CC, Jansonius NM, Hooymans JMM, Cornelissen FW. Automated morphometry of the visual pathway in primary open-angle glaucoma. *Invest Ophthalmol Vis Sci*. 2011;52:2758–2766.
11. Gupta N, Greenberg G, de Tilly LN, Gray B, Polemidiotis M, Yucel YH. Atrophy of the lateral geniculate nucleus in human glaucoma detected by magnetic resonance imaging. *Br J Ophthalmol*. 2009;93:56–60.
12. Prins D, Hanekamp S, Cornelissen FW. Structural brain MRI studies in eye diseases: are they clinically relevant? A review of current findings. *Acta Ophthalmol*. 2016;94:113–121.
13. Lawlor M, Danesh-Meyer H, Levin LA, Davagnanam I, De Vita E, Plant GT. Glaucoma and the brain: trans-synaptic degeneration, structural change, and implications for neuroprotection. *Surv Ophthalmol*. 2017;63:296–306.
14. Yücel YH, Zhang Q, Weinreb RN, Kaufman PL, Gupta N. Effects of retinal ganglion cell loss on magno-, parvo-, koniocellular pathways in the lateral geniculate nucleus and visual cortex in glaucoma. *Prog Retin Eye Res*. 2003;22:465–481.
15. Frezzotti P, Giorgio A, Motolese I, et al. Structural and functional brain changes beyond visual system in patients with advanced glaucoma. *PLoS One*. 2014;9:e105931.
16. Frezzotti P, Giorgio A, Toto F, De Leucio A, De Stefano N. Early changes of brain connectivity in primary open angle glaucoma. *Hum Brain Mapp*. 2016;37:4581–4596.
17. Boucard CC, Hanekamp S, Curcic-Blake B, Ida M, Yoshida M, Cornelissen FW. Neurodegeneration beyond the primary visual pathways in a population with a high incidence of normal-pressure glaucoma. *Ophthalmic Physiol Opt*. 2016; 36:344–353.
18. Kaushik M, Graham SL, Wang C, Klistorner A. A topographical relationship between visual field defects and optic radiation changes in glaucoma. *Invest Ophthalmol Vis Sci*. 2014;55: 5770–5775.
19. Sidek S, Ramli N, Rahmat K, Ramli NM, Abdulrahman F, Tan LK. Glaucoma severity affects diffusion tensor imaging (DTI) parameters of the optic nerve and optic radiation. *Eur J Radiol*. 2014;83:1437–1441.
20. Zikou AK, Kitsos G, Tzarouchi LC, Astrakas L, Alexiou GA, Argyropoulou MI. Voxel-based morphometry and diffusion tensor imaging of the optic pathway in primary open-angle glaucoma: a preliminary study. *Am J Neuroradiol*. 2012;33: 128–134.

21. Tellouck L, Durieux M, Coupé P, et al. Optic radiations microstructural changes in glaucoma and association with severity: a study using 3 Tesla-magnetic resonance diffusion tensor imaging. *Invest Ophthalmol Vis Sci*. 2016;57:6539–6547.
22. Zhou W, Muir ER, Chalfin S, Nagi KS, Duong TQ. MRI study of the posterior visual pathways in primary open angle glaucoma. *J Glaucoma*. 2017;26:173–181.
23. Nucci C, Mancino R, Martucci A, et al. 3-T diffusion tensor imaging of the optic nerve in subjects with glaucoma: correlation with GDx-VCC, HRT-III and Stratus optical coherence tomography findings. *Br J Ophthalmol*. 2012;96:976–980.
24. Bolacchi F, Garaci FG, Martucci A, et al. Differences between proximal versus distal intraorbital optic nerve diffusion tensor magnetic resonance imaging properties in glaucoma patients. *Invest Ophthalmol Vis Sci*. 2012;53:4191–4196.
25. Chen Z, Lin F, Wang J, et al. Diffusion tensor magnetic resonance imaging reveals visual pathway damage that correlates with clinical severity in glaucoma. *Clin Exp Ophthalmol*. 2013;41:43–49.
26. Michelson G, Engelhorn T, Wärntges S, El Rafei A, Hornegger J, Doerfler A. DTI parameters of axonal integrity and demyelination of the optic radiation correlate with glaucoma indices. *Graefe's Arch Clin Exp Ophthalmol*. 2013;251:243–253.
27. Li M, Ke M, Song Y, Mu K, Zhang H, Chen Z. Diagnostic utility of central damage determination in glaucoma by magnetic resonance imaging: an observational study. *Exp Ther Med*. 2019;17:1891–1895.
28. Song X, Puyang Z, Chen A, et al. Diffusion tensor imaging detects microstructural differences of visual pathway in patients with primary open-angle glaucoma and ocular hypertension. *Front Hum Neurosci*. 2018;12:426.
29. You Y, Joseph C, Wang C, et al. Demyelination precedes axonal loss in the transneuronal spread of human neurodegenerative disease. *Brain*. 2019;142:426–442.
30. El-Rafei A, Engelhorn T, Wärntges S, Dörfler A, Hornegger J, Michelson G. Glaucoma classification based on visual pathway analysis using diffusion tensor imaging. *Magn Reson Imaging*. 2013;31:1081–1091.
31. Murai H, Suzuki Y, Kiyosawa M, Tokumaru AM, Ishii K, Mochizuki M. Positive correlation between the degree of visual field defect and optic radiation damage in glaucoma patients. *Jpn J Ophthalmol*. 2013;57:257–262.
32. Wang MY, Wu K, Xu JM, et al. Quantitative 3-T diffusion tensor imaging in detecting optic nerve degeneration in patients with glaucoma: association with retinal nerve fiber layer thickness and clinical severity. *Neuroradiology*. 2013;55:493–498.
33. Garaci FG, Bolacchi F, Cerulli A, et al. Optic nerve and optic radiation neurodegeneration in patients with glaucoma: in vivo analysis with 3-T diffusion-tensor MR imaging. *Radiology*. 2009;252:496–501.
34. Engelhorn T, Michelson G, Waerntges S, Struffert T, Haider S, Doerfler A. Diffusion tensor imaging detects rarefaction of optic radiation in glaucoma patients. *Acad Radiol*. 2011;18:764–769.
35. Lu P, Shi L, Du H, et al. Reduced white matter integrity in primary open-angle glaucoma: a DTI study using tract-based spatial statistics. *J Neuroradiol*. 2013;40:89–93.
36. Omodaka K, Murata T, Sato S, et al. Correlation of magnetic resonance imaging optic nerve parameters to optical coherence tomography and the visual field in glaucoma. *Clin Exp Ophthalmol*. 2014;42:360–368.
37. Jeurissen B, Leemans A, Tournier JD, Jones DK, Sijbers J. Investigating the prevalence of complex fiber configurations in white matter tissue with diffusion magnetic resonance imaging. *Hum Brain Mapp*. 2013;34:2747–2766.
38. Wedeen VJ, Hagmann P, Tseng WYI, Reese TG, Weisskoff RM. Mapping complex tissue architecture with diffusion spectrum magnetic resonance imaging. *Magn Reson Med*. 2005;54:1377–1386.
39. Tuch DS, Reese TG, Wiegell MR, Wedeen VJ. Diffusion MRI of complex neural architecture. *Neuron*. 2003;40:885–895.
40. Tournier JD, Calamante F, Gadian DG, Connelly A. Direct estimation of the fiber orientation density function from diffusion-weighted MRI data using spherical deconvolution. *Neuroimage*. 2004;23:1176–1185.
41. Jensen JH, Helpern JA, Ramani A, Lu H, Kaczynski K. Diffusional kurtosis imaging: the quantification of non-Gaussian water diffusion by means of magnetic resonance imaging. *Magn Reson Med*. 2005;53:1432–1440.
42. Zhang H, Schneider T, Wheeler-Kingshott CA, Alexander DC. NODDI: practical in vivo neurite orientation dispersion and density imaging of the human brain. *Neuroimage*. 2012;61:1000–1016.
43. Raffelt D, Tournier JD, Rose S, et al. Apparent fibre density: a novel measure for the analysis of diffusion-weighted magnetic resonance images. *Neuroimage*. 2012;59:3976–3994.
44. Tournier JD, Calamante F, Connelly A. Robust determination of the fibre orientation distribution in diffusion MRI: non-negativity constrained super-resolved spherical deconvolution. *Neuroimage*. 2007;35:1459–1472.
45. Raffelt DA, Tournier JD, Smith RE, et al. Investigating white matter fibre density and morphology using fixel-based analysis. *Neuroimage*. 2017;144:58–73.
46. Mito R, Raffelt D, Dhollander T, et al. Fibre-specific white matter reductions in Alzheimer's disease and mild cognitive impairment. *Brain*. 2018;March:888–902.
47. Veraart J, Fieremans E, Novikov DS. Diffusion MRI noise mapping using random matrix theory. *Magn Reson Med*. 2016;76:1582–1593.
48. Andersson JLR, Skare S, Ashburner J. How to correct susceptibility distortions in spin-echo echo-planar images: application to diffusion tensor imaging. *Neuroimage*. 2003;20:870–888.
49. Andersson JLR, Sotiropoulos SN. An integrated approach to correction for off-resonance effects and subject movement in diffusion MR imaging. *Neuroimage*. 2016;125:1063–1078.
50. Jenkinson M, Beckmann CF, Behrens TEJ, Woolrich MW, Smith SM. FSL. *Neuroimage*. 2012;62:782–790.
51. Dhollander T, Raffelt D, Connelly A. Unsupervised 3-tissue response function estimation from single-shell or multi-shell diffusion MR data without a co-registered T1 image. In: *ISMRM Workshop on Breaking the Barriers of Diffusion MRI*. Vol. 5. Concord, CA: ISMRM; 2016.
52. Jeurissen B, Tournier JD, Dhollander T, Connelly A, Sijbers J. Multi-tissue constrained spherical deconvolution for improved analysis of multi-shell diffusion MRI data. *Neuroimage*. 2014;103:411–426.
53. Raffelt D, Tournier JD, Fripp J, Crozier S, Connelly A, Salvado O. Symmetric diffeomorphic registration of fibre orientation distributions. *Neuroimage*. 2011;56:1171–1180.
54. Raffelt D, Tournier JD, Crozier S, Connelly A, Salvado O. Reorientation of fiber orientation distributions using apodized point spread functions. *Magn Reson Med*. 2012;67:844–855.
55. Raffelt DA, Smith RE, Ridgway GR, et al. Connectivity-based fixel enhancement: whole-brain statistical analysis of diffusion MRI measures in the presence of crossing fibres. *Neuroimage*. 2015;117:40–55.
56. Smith RE, Tournier JD, Calamante F, Connelly A. SIFT: spherical-deconvolution informed filtering of tractograms. *Neuroimage*. 2013;67:298–312.

Investigative Ophthalmology & Visual Science

57. Bürgel U, Amunts K, Hoemke L, Mohlberg H, Gilsbach JM, Zilles K. White matter fiber tracts of the human brain: three-dimensional mapping at microscopic resolution, topography and intersubject variability. *Neuroimage*. 2006;29:1092–1105.
58. Veraart J, Sijbers J, Sunaert S, Leemans A, Jeurissen B. Weighted linear least squares estimation of diffusion MRI parameters: strengths, limitations, and pitfalls. *Neuroimage*. 2013;81:335–346.
59. Smith SM, Nichols TE. Threshold-free cluster enhancement: addressing problems of smoothing, threshold dependence and localisation in cluster inference. *Neuroimage*. 2009;44:83–98.
60. Hodapp E, Parrish RK II, Anderson DR. *Clinical Decisions in Glaucoma*. St. Louis, MO: C.V. Mosby; 1993:52–61.
61. Burda JE, Sofroniew MV. Reactive gliosis and the multicellular response to CNS damage and disease. *Neuron*. 2014;81:229–248.
62. Li K, Lu C, Huang Y, Yuan L, Zeng D, Wu K. Alteration of fractional anisotropy and mean diffusivity in glaucoma: novel results of a meta-analysis of diffusion tensor imaging studies. *PLoS One*. 2014;9:e97445.
63. Catani M, Jones DK, Donato R, Ffytche DH. Occipito-temporal connections in the human brain. *Brain*. 2003;126:2093–2107.
64. Sarubbo S, De Benedictis A, Milani P, et al. The course and the anatomo-functional relationships of the optic radiation: a combined study with "post mortem" dissections and "in vivo" direct electrical mapping. *J Anat*. 2015;226:47–59.
65. Mandelstam SA. Challenges of the anatomy and diffusion tensor tractography of the Meyer loop. *Am J Neuroradiol*. 2012;33:1204–1210.
66. Giorgio A, Zhang J, Costantino F, De Stefano N, Frezzotti P. Diffuse brain damage in normal tension glaucoma. *Hum Brain Mapp*. 2017;541:532–541.
67. Dai H, Yin D, Hu C, et al. Whole-brain voxel-based analysis of diffusion tensor MRI parameters in patients with primary open angle glaucoma and correlation with clinical glaucoma stage. *Neuroradiology*. 2013;55:233–243.
68. Garway-Heath DF, Quartilho A, Prah P, Crabb DP, Cheng Q, Zhu H. Evaluation of visual field and imaging outcomes for glaucoma clinical trials (an American Ophthalomological Society thesis). *Trans Am Ophthalmol Soc*. 2017;115:T4.
69. Nucci C, Martucci A, Giannini C, Morrone LA, Bagetta G, Mancino R. Neuroprotective agents in the management of glaucoma. *Eye*. 2018;32:938–945.
70. Rusciano D, Pezzino S, Mutolo MG, Giannotti R, Librando A, Pescosolido N. Neuroprotection in glaucoma: old and new promising treatments. *Adv Pharmacol Sci*. 2017;2017:4320408.
71. Venugopalan P, Wang Y, Nguyen T, Huang A, Muller KJ, Goldberg JL. Transplanted neurons integrate into adult retinas and respond to light. *Nat Commun*. 2016;7:1–9.

Investigative Ophthalmology & Visual Science